Materials & Design 254 (2025) 114148

Contents lists available at ScienceDirect

Materials & Design

journal homepage: www.elsevier.com/locate/matdes

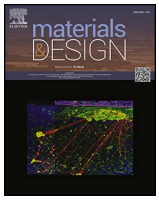

Ceramic fused filament fabrication (CF^3) of zirconia implants by using flexible, partially water-soluble binder systems

Ralf Eickhoff [a,*], Dorit Nötzel [a], Gülsenem Oral [a], Mark Scholz [a], Thomas Hanemann [a,b]

[a] Institute for Applied Materials, Karlsruhe Institute of Technology, Hermann-von-Helmholtz-Platz 1, D-76344 Eggenstein-Leopoldshafen, Germany
[b] Department of Microsystems Engineering, University Freiburg, Georges-Koehler-Allee 102, D-79110 Freiburg, Germany

ARTICLE INFO

Keywords:
3D printing
Additive manufacturing
CF^3
Zirconia
Water-soluble binder
Implants

ABSTRACT

Ceramic Fused Filament Fabrication offers a simple and cost-effective method to manufacture personalized ceramic implants. However, the lack of flexibility in highly filled filaments and the reduced accuracy compared to alternative additive manufacturing techniques limit the method's widespread implementation. Therefore, an eco-friendly partially water-soluble binder system containing polyethylene glycol (PEG), poly(vinylbutyral) (PVB), and poly(methylmethacrylat) (PMMA) was investigated, along with the influence of the two additives acetyltributylcitrate (ATBC) and lauric acid (LA). The created feedstocks were characterized by comprehensive rheological analysis, which included capillary rheology and dynamic mechanical analysis. The production of filaments with a solid content of 50 vol% was successfully achieved, demonstrating exceptional flexibility and flow properties. Following the debinding and sintering processes, the optimal feedstock systems enabled the fabrication of defect-free components with a high level of detail and relative densities up to 100 %.

1. Introduction

Additive manufacturing (AM) is poised to become the predominant method of producing medical applications, such as protheses, surgical models, 3D scaffolds, and even organic tissues [1–4]. The ability to manufacture personalized solutions can improve the quality of life of patients after a disease, an accident, or at a high age. In addition, AM allows faster production and with reduced costs compared to traditional manufacturing methods [5], thereby enabling widespread distribution beyond the confines of wealthy industrialized nations. Ceramics, in particular, stand to benefit significantly, as their current methods of production present challenges in efficiently producing small quantities of parts with complex geometries at a competitive cost [6].

Additive manufacturing of ceramics has evolved significantly since its initial introduction in the 1990s. Beginning with selective laser sintering (SLS) [7], there are now several different approaches to print ceramics. The most prevalent AM technologies include powder bed-based methods such as selective laser sintering (SLS) or binder jetting (BJ), slurry-based techniques like stereolithography (SLA) or digital light processing (DLP), and bulk solid-based approaches like laminated object manufacturing (LOM) or ceramic fused filament fabrication (CF^3) [8]. These methods differ in terms of achievable resolution, processing time, environmental impact, and cost. Powder-based 3D printing technologies provide a high degree of geometric design flexibility, they are constrained in terms of resolution, density, and mechanical performance. Slurry-based printing technologies, SLA, DLP, and material jetting (MJ), provide the highest resolution, making them well suited for manufacturing ceramic implants. These technologies have been successfully used to produce dental prostheses [9], dental implants [10,11], and complex-shaped bone implants for splicing bones and soft tissues [12]. However, the stability of the ceramic bulk photosensitive monomer resins, the slow debinding process, and the high costs of the equipment and the resins are still current limitations [8]. Regarding these issues, ceramic bulk solid-based printing technologies can be a viable alternative. While LOM is constrained to rudimentary structures and yields a substantial amount of waste, CF^3 provides an opportunity to upgrade cost-effective commercial Fused Filament Fabrication (FFF) printers in a simple and economical manner, significantly reducing capital investment. Additionally, it allows the processing of a wide range of materials [13–18], including metals [19] and the combination of different materials within the same object [20]. This presents the opportunity to manufacture functionally graded materials, thereby

* Corresponding author.
E-mail addresses: ralf.eickhoff@kit.edu (R. Eickhoff), dorit.noetzel@kit.edu (D. Nötzel), ufyef@student.kit.edu (G. Oral), ugxfi@student.kit.edu (M. Scholz), thomas.hanemann@kit.edu, thomas.hanemann@imtek.uni-freiburg.de (T. Hanemann).

https://doi.org/10.1016/j.matdes.2025.114148
Received 2 April 2025; Received in revised form 15 May 2025; Accepted 23 May 2025
Available online 24 May 2025

enabling the selection of the most suitable material for each load type within the implant. Nevertheless, CF^3 is still in the early stages of development. The present challenges encompass the limited flexibility of filled filaments, the interlayer connectivity of the printed components, printing without generating voids, the debinding process, and the suboptimal level of detail [21–24]. However, there are reports of the fabrication of ceramic parts with details measuring between 80 and 90 μm [22].

As with related ceramic injection molding (CIM), CF^3 follows a strict process chain to ensure the absence of defects in the final product. The process can be subdivided into five steps: (1) characterization, selection, and compounding of the ceramic powder and the polymers to the so-called feedstock; (2) extrusion of filaments; (3) printing of components using CF^3; (4) debinding; and (5) sintering. The selection of polymers as binder constitutes a critical step in the process, perhaps even the most important. First, the polymers must ensure sufficient flexibility of the filaments for optimal usability. Second, the selected polymers must enable the shaping of the desired parts at low temperatures without defects and retain the integrity of the printed component. Third, the polymers must be capable of being removed during the debinding process without leaving any defects or organic residues in the produced parts. Due to the wide range of tasks involved, a variety of polymers and additives are used, depending on the debinding method selected. Combined solvent and thermal debinding is frequently utilized due to the low number of defects in the final parts and the cost-effective equipment. This two-step process involves the removal of the soluble base polymer in a solvent, followed by the combustion of the backbone polymer in a second step. Solvent debinding is typically carried out using organic solvents [25–27]. However, there is ongoing work to replace potentially hazardous organic solvents with water in order to reduce costs and environmental impact [16,28]. The final step to obtain dense zirconia implants is sintering. During this process, diffusion mechanisms result in rearrangement, particle movement, and mass transport. These mechanisms reduce the surface energy by forming solid bonds between powder particles. Additionally, some diffusion processes result in a reduction in porosity, leading to the shrinkage and densification of the parts. The microstructure can be adjusted by varying the sintering temperature and time, thereby producing the desired material properties.

2. Materials and methods

2.1. Material selection

2.1.1. Zirconia powder (ZrO_2)

Due to their elevated mechanical load and the requisite durability, medical zirconia implants must meet stringent requirements [29] to prevent the need for subsequent surgical interventions. Therefore, precise knowledge about the powder properties is necessary to adapt the polymeric binder to the selected powder for controlling the flow properties of the feedstocks. The submicron-sized yttria-stabilized zirconia (TZ-3YS-E, Tosoh Corp., Tokio, Japan), which is suitable for medical applications, was selected. The particle density was measured by helium pycnometry (AccuPyc II 1340, Micromeritics Instr. Corp., Norcross, GA, USA), the specific surface area (SSA) was determined via the BET method (Gemini VII 2390, Micromeritics Instr. Corp., Norcross, GA, USA), and the particle size distribution was measured by laser diffraction (LA-950 Horiba Ltd., Kyoto, Japan). Table 1 provides a comprehensive overview of the measured as well as the vendor-provided particle properties. As illustrated in Fig. 1, the missmatch in particle size is likely attributable to the presence of agglomerates (Fig. 1a) and aggregates (Fig. 1b) of the primary particles.

Table 1
Particle properties.

TZ-3YS-E	Density (g/cm^3)	D_{10} (μm)	D_{50} (μm)	D_{90} (μm)	SSA (m^2/g)
Vendor	6.05	–	0.090	–	7.0
Measured	6.04	0.150	0.396	1.715	6.6

2.1.2. Thermoplastic binder system

The thermoplastic binder plays a critical role in ensuring the quality of the products. It has to ensure a homogeneous distribution of the powder and a low viscosity of the feedstocks. Additionally, it provides the necessary flexibility to the filaments, ensuring their usability, and keeps the powder particles in their shaped form until the sintering phase. Furthermore, the binder must be completely removable and must not leave any residue behind. To fulfill these comprehensive requirements, the thermoplastic is composed of at least four distinct components. The high-viscosity backbone polymers poly(vinyl butyral) (PVB, Mowital 30H, Kuraray Europe GmbH, Frankfurt, Germany) and poly(methyl methacrylate) (PMMA, Degalan G7E, Roehm GmbH, Darmstadt, Germany) provide strength of the filaments and of the printed parts during the first debinding step in water. The low molecular weight and water-soluble base polymer polyethylene glycol (PEG 4,000, C. Roth GmbH Co. KG, Karlsruhe, Germany) provides low viscosity of the feedstocks and defect-free debinding. The polymer chains are sufficiently short to exhibit low viscosity, thereby enhancing the printing properties, yet sufficiently long to prevent binder separation. Acetyltributyl citrate (ATBC, Sigma Aldrich, St. Louis, USA) is a widely used additive that functions as a environmentally friendly substitute for phthalates. It plays a crucial role in ensuring the flexibility of filaments by acting as a plasticizer. Lauric acid (LA, Sigma Aldrich, St. Louis, MO, USA) functions as a dispersant, contributing to the optimized flow properties of the feedstocks while also demonstrating the capacity to enhance filament flexibility [30,31]. In addition to the manufacturer's specifications, the density of the organic components were characterized by helium pycnometry (AccuPyc II 1340, Micromeritics Instr. Corp., Norcross, GA, USA). The thermal behavior was analyzed by Thermogravimetric Analysis (TGA) and Differential Scanning Calorimetry (DSC) using the Netzsch STA 449 F3 Jupiter (Netzsch GmbH & Co. KG, Selb, Germany) in synthetic air. The measured properties are listed in Table 2. The softening and decomposition temperatures were derived from the TGA-DSC measurements.

2.1.3. Feedstock compositions

To achieve the desired densities of the manufactured parts after sintering with minimal shrinkage, it is essential to use zirconia powder feedstocks with a high solid content. However, a high solid loading increases the viscosity of the feedstocks and can reduce the flexibility of the filaments. Accordingly, a solid load of 50 vol% was selected for all feedstock systems to reconcile these objectives. Two distinct binder compostions were examined in this work: PVB/PEG and PMMA/PVB/PEG (Table 3). Previous studies have demonstrated that PVB tends to deform and swell during solvent debinding in water [31]. Therefore, the addition of water-resistant PMMA was investigated to prevent potential defects in this step. PEG 4,000 was utilized as the base polymer. The ATBC content was set at 16.7 vol% of the binder for all feedstocks, and the lauric acid concentration was set at 1.15 mg/m^2. This was based on the specific surface area of the zirconia. The objective was to form at least one monolayer on the particles in order to reduce the friction between them [32]. This guaranteed complete ceramic particle surface coverage. The calculated value for lauric acid was then subtracted from the content of the base polymer PEG. The exact feedstock compositons can be found in the next section.

2.2. Compounding and extrusion

Compounding of the feedstocks was carried out on a torque recording mixer-kneader (W50-EHT, Brabender GmbH, Duisburg, Germany). The applied parameters are listed in Table 4. The blade's rotating speed was set to 30 rpm, which is equivalent to a shear rate of 2 to 36 1/s

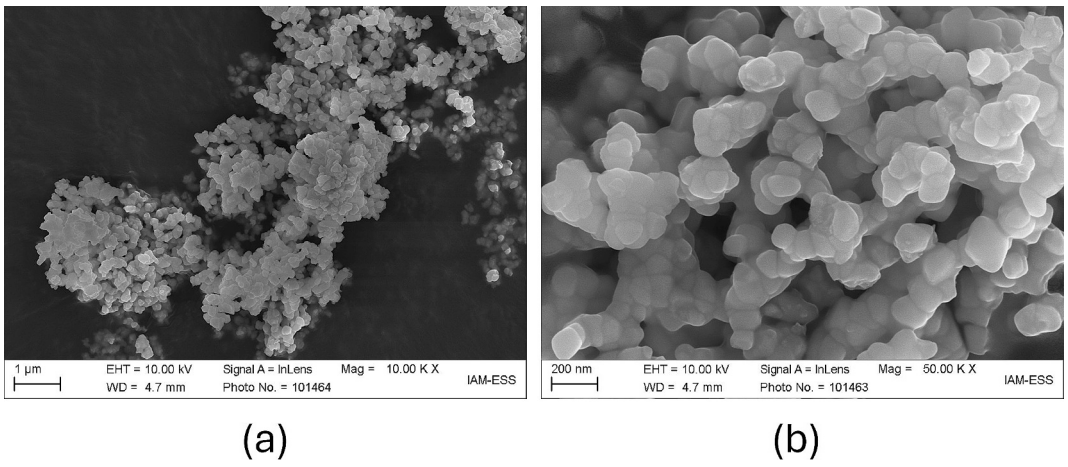

Fig. 1. SEM-images of the used zirconia TZ-3YS-E illustrating the particles morphology; while agglomerates can be observed in (a), the higher-magnitude SEM image in (b) indicates the presence of aggregates.

Table 2
Properties of the binder components used (T_S: softening temperature, T_D: decomposition temperature).

Component	Density (g/cm^3)	M_W (g/mol)	T_S (°C)	T_D (°C)
PMMA G7E	1.18	159,000[V]	106	252
PVB 30H	1.11	32,000–35,000[V]	64	286
PEG 4,000	1.22	3,500–4,500[V]	55	209
Lauric Acid	0.95	200[V]	50	184
ATBC	1.05	402[V]	−80[V]	226

V: Vendor's data sheet.

Table 3
Overview of the binder compositions investigated.

Combination	Backbone polymer	Base polymer	Plasticizer	Dispersant
PVB/PEG	PVB 30H	PEG 4,000	ATBC	Lauric acid
PMMA/PVB/PEG	PMMA G7E/PVB 30H	PEG 4,000	ATBC	Lauric acid

[33]. The compounding temperatures were contingent on the glass transition temperature of the utilized backbone polymers. In order to avoid the inhomogeneities observed in previous studies [34] due to the use of large PMMA pellets, a new method was employed. Smaller PMMA granules were produced using a capillary rheometer (Rheograph 25, Göttfert Werkstoff-Prüfmaschinen GmbH, Buchen, Germany) and subsequently pelletized using an impact mill (Granulator 1514, Rapid Germany, Kleinostheim, Germany). Furthermore, a compounding time of two hours was applied to break the agglomerates and ensure the homogeneity of the feedstocks. Otherwise, the agglomerates may result in brittle filaments and printing defects. After compounding, the feedstocks were extruded into filaments by using a single screw filament extruder (Noztek pro HT, Noztek, Shoreham, UK). The parameters utilized are depicted in Table 4. The desired filament diameter was 2.85 mm instead of the common 1.75 mm. Due to its larger diameter relative to the volume of the fed material, it exhibits reduced sensitivity to diameter fluctuations, resulting in smaller fluctuations in the volume of the printed parts. The filaments were then wound onto a spool by using a winder (Noztek Filament Winder 1.0, Noztek, Shoreham, UK).

2.3. Rheological characterization

Viscosity measurements were carried out using a high-pressure capillary rheometer (Rheograph 25, Göttfert Werkstoff-Prüfmaschinen GmbH, Buchen, Germany). The Weissenberg-Rabinowitsch correction was applied to enhance the precision of the measured values. All investigated systems were compared using the same parameters:

- Temperature: 160 °C,
- Capillary length and diameter: 30 and 1 mm,
- Shear rate range: 1 to 3000 1/s.

Furthermore, and in continuation of a method introduced in previous work [31] to quantify the flexibility of the filaments, the temperature-dependent viscoelastic behavior was characterized by oscillatory measurements in the temperature sweep (TS) mode by using a dynamic mechanical analyzer (DMA 242 E Artemis, Netzsch GmbH & Co. KG, Selb, Germany) equipped with a dual cantilever sample holder (2 × 16 mm free bending length). The following parameters were employed:

- Temperature: 20–50 °C,
- Frequency: 0.5 Hz,
- Amplitude: 50 µm,

Table 4
Overview of the binder compositions, compounding and extrusion parameters used.

PMMA/PVB/PEG/ATBC (vol.%)	Compounding time (h)	Compounding temperature (°C)	Extrusion temperature (°C)	Nozzle size (mm)
0/40/43.3/16.7	2	125	90	2.95
0/35/48.3/16.7	2	125	85	2.95
0/30/53.3/16.7	2	125	85	2.95
10/30/43.3/16.7	2	160	120	2.95
10/25/48.3/16.7	2	160	115	2.95
10/20/53.3/16.7	2	160	115	2.95
15/30/38.3/16.7	2	160	120	2.95
20/30/33.3/16.7	2	160	125	2.95

- Pre-force: 0.1 N.

2.4. Fused filament fabrication

Printing was carried out on a commercial but slightly modified FFF printer (German RepRap x350pro, Feldkirchen, Germany). The printer is depicted in Fig. 2. The original extruder was replaced by a Bondtech QR Extruder (Värnamo, Sweden) with Dual-Drive technology and an E3D V6 Hotend for 2.85 mm filaments (Oxfordshire, UK). According to the vendor, this extruder offers higher precision and reliability. To improve the accuracy of complex parts, part surface ventilation was installed. For enhanced adhesion and removal of the printed parts, the print bed was covered with polyethylene-coated spring steel. Ultimaker Cura (V 5.4.0) was used for slicing. For subsequent characterization such as debinding behavior and density, ten cubic specimens (10 mm × 10 mm × 2.5 mm) were printed. A sketch can be found in [35], were printed for subsequent characterization. The printing parameters for the cubic specimens are listed in Table 5. Deviations and feedstock-specific parameters such as the temperature are described in the respective section. Furthermore, a variety of nozzle sizes (0.15 mm, 0.25 mm, 0.3 mm, 0.4 mm, 0.6 mm, and 0.8 mm) were assessed to evaluate the potential of the feedstocks for printing small and large parts.

2.5. Debinding and sintering

The debinding process was executed in a two-step method. Initially, PEG was removed in water for 24 h at 25 °C, a step that generates open pores. This procedure reduces the thermal debinding time and prevents debinding-related defects, such as blisters and cracks. Subsequently, the components were dried overnight in a vacuum drying furnace at 30 °C to remove any residual water. Thermal debinding was then conducted at a heating rate of 0.2 K/min up to 500 °C to remove the remaining polymers (HT5/28, Carbolite, Neuhausen, Germany). Finally, the samples were sintered at a heating rate of 5 K/min, a maximum temperature of 1450 °C, and a sintering time of 2 h (HTF17/5, Carbolite, Neuhausen, Germany).

2.6. Characterization of sintered samples

The density of the sintered samples was measured by using the Archimedes principle (Secura 225D-1S equipped with YDK 01, Sartorius Lab Instruments GmbH & Co. KG, Göttingen, Germany). To calculate the relative density, the measured pycnometer density of the zirconia powder was used as a basis. The microstructure and potential defects were analyzed through SEM (Supra 55 FE-SEM, Zeiss, Oberkochen, Germany). For microscopic analysis, the samples were embedded, ground with different grinding wheels (70 μm until planarity, 40 μm for 30 s, and 10 μm for 2 min), and polished with diamond paste and lubricant (6 μm and 3 μm, each for 30 min).

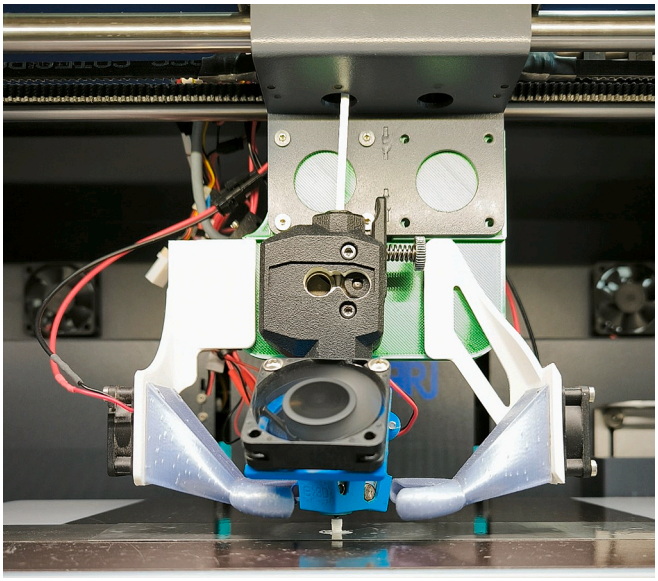

Fig. 2. Modified FFF printer x350 pro.

Table 5
Overview of the printing parameters used for the cubic specimens.

Parameter	Value	Parameter	Value
Infill density	105 %	Layer height	0.1 mm
Infill angle offset	90°	Nozzle size	0.4 mm
Infill pattern	Rectilinear	Number of walls	2
Infill overlap	0.2 mm	Printing speed	8 mm/s

3. Results and discussion

3.1. Compounding

As described in [32], the torque curve during compounding can usually be subdivided into three phases: the filling phase, the mixing phase, and the equilibrium phase. In the first state, all components are inserted into the mixing chamber. During the second state, the break of the particle agglomerates and friction between the particles occurs, resulting in a strong but short peak in torque. After the primary particles, the aggregates and the agglomerates are wetted by the organic binder components, the torque decreases drastically. In the final phase, an equilibrium between agglomeration and deagglomeration occurs, resulting in a relatively constant torque. Fig. 3a and b illustrates the time-dependent torque curves depending on the binder composition. An increased PEG content led to a decrease in torque, attributable to the shorter PEG chains when compared to the longer PVB and PMMA chains. This results in a lower entanglement between the polymer chains, leading to reduced friction. The increase in torque due to higher PMMA content is similarly attributable to the five times higher molecular weight of PMMA compared to PVB. Although the torque appears to be generally lower for the PMMA-based feedstocks, this is distorted by the higher compounding temperature of 160 °C (compared to the 125 °C of the PMMA-free feedstocks).

3.2. Rheological properties

3.2.1. Capillary rheology

As indicated in the torque curves in the previous section, the viscosity of the feedstocks decreases with increasing PEG content (Fig. 4a). Furthermore, a shear thinning behavior was observed for every feedstock. According to the extant literature, the range of the shear rate for FFF is between 40 and 450 s^{-1} [31,36,37], contingent upon the utilized binder system and the printing parameters, such as nozzle size or printing speed [38]. In this range, all PMMA-free feedstocks remain below a viscosity of 1000 Pas, which is a reliable indicator for determining the feasibility of processing the feedstock. The addition of high-molecular weight PMMA increased the viscosity significantly (Fig. 4b), leading to a smaller range of feasible shear rates.

3.2.2. DMA

As indicated by previous studies, the storage modulus is a reliable indicator of filament flexibility [31]. Values below 600 MPa at a temperature of 25 °C demonstrate sufficient flexibility for optimal filament usability. Fig. 5a shows the temperature-dependent storage modulus of the PMMA-free feedstocks. All three materials remain below the limit, exhibiting excellent flexibility. However, the addition of PMMA and a higher PEG content increased the storage modulus significantly (Fig. 5b). While filaments with 10 vol% PMMA in combination with

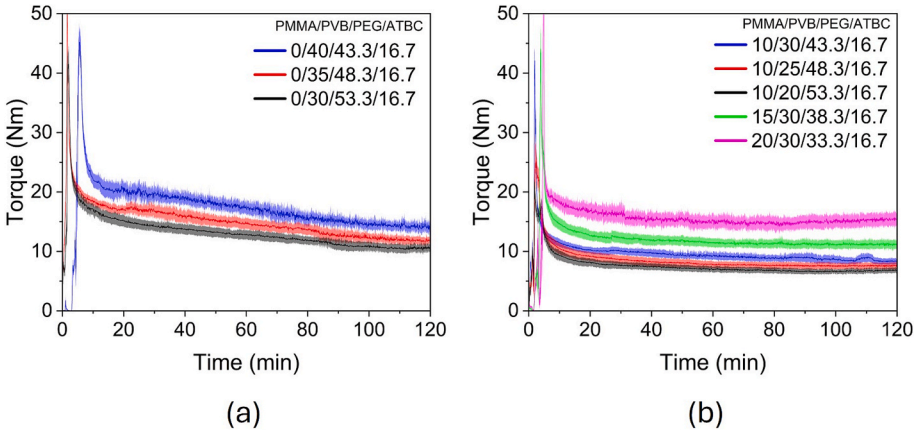

Fig. 3. Compounding of feedstocks made of PMMA/PVB/PEG/ATBC at (a) 125 °C and (b) 160 °C. A higher temperature is necessary to dissolve the PMMA granules in the feedstocks.

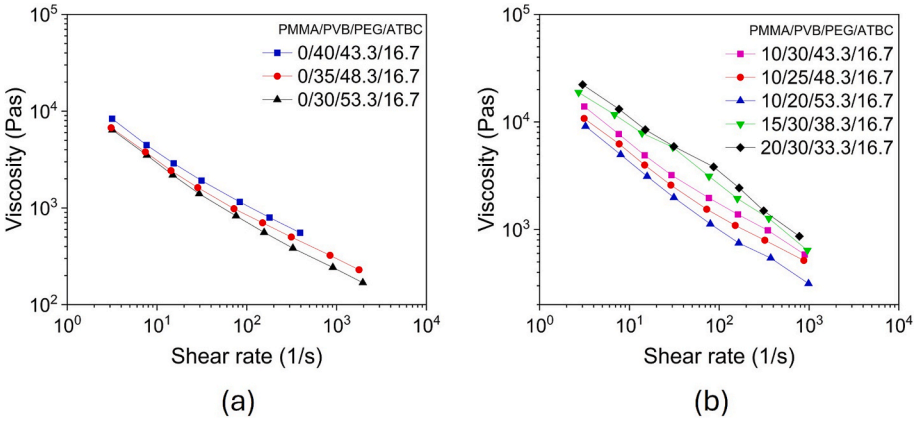

Fig. 4. Capillary rheology of feedstocks made of PMMA/PVB/PEG/ATBC at 160 °C; (a) PMMA-free feedstocks and (b) PMMA-based feedstocks.

43.3 vol% PEG demonstrated flexibility, increasing the PEG content and decreasing the PVB content resulted in increased stiffness. This is likely attributable to the excellent bonding of the ATBC molecules to the PVB chains, leading to plasticization of the feedstock. In practice, however, sufficient flexibility was also achieved with filaments containing 15 or 20 vol% PMMA. This suggests that the storage modulus is not the sole criterion for assessing flexibility. Therefore, the viscous behavior of the filaments was also examined. Fig. 5c and d illustrate the time-dependent tan δ, which is the ratio of the viscous modulus (G'') and the storage modulus (G') of a polymer ($\tan\delta = G''/G'$). It is evident that an increase in PEG content leads to a reduced viscous behavior of the feedstock. Additionally, both feedstocks with a high PMMA content exhibited the highest tan δ values among the PMMA-based feedstocks, likely due to their lower PEG content compared to the other feedstocks. Therefore, the flexible behavior must be a consequence of the viscous deformation of the filaments. In general, the use of PEG tends to have a negative impact on the elastic and viscous behavior of the materials. This is likely attributable to the weak bonding of the ATBC molecules to the PEG chains. Based on these findings, it can be concluded that a tan δ value of approximately 0.2 at 25 °C is a reliable indicator for assessing the flexibility of the filaments. A higher value indicates a flexible filament, while a lower value indicates a stiff filament. However, it is possible that the flexibility of the filaments is underestimated due to inhomogeneities resulting from agglomerates present in the feedstocks. Therefore, further investigation and assessment of the developed feedstocks is necessary. This can be accomplished by compounding at higher shear rates, for instance using double screw extruders.

3.3. Fused filament fabrication

Ten cubic specimens, dental implants and a chess piece with a complex geometry were printed to assess the printing properties of the respective feedstocks. The printing temperatures of the feedstocks and the potential nozzle sizes that could be utilized are listed in Table 6. According to the measured shear viscosities, the PMMA-free feedstocks could be printed at lower temperatures compared to the PMMA-based feedstocks. An increase in PMMA content resulted in elevated temperatures, although this increase was only moderate given the high softening temperature of PMMA compared to the other binder components. Only for the two feedstocks with 15 vol% and 20 vol%, high printing temperatures of 180 °C and 200 °C were necessary. These temperatures partly exceed the decomposition temperature of lauric acid. However, due to the brief exposure of the feedstocks to the heated nozzle, this typically does not have any adverse effects on the printed parts. The influence of the PMMA content was also evident in the printing bed temperatures. Due to the low viscosity of the PMMA-free feedstocks, the lower layers of the samples showed deformations at bed temperatures above 30 °C (Fig. 6), which was not an issue with the PMMA-based feedstocks. The difference in shear viscosity was also evident in the possible nozzle diameters. While 0.15 mm was feasible for the low-viscosity feedstocks, 0.3 mm was the lower limit for continuous and defect-free printing with PMMA-based feedstocks. The use of large nozzle diameters up to 0.8 mm was feasible for all feedstocks.

Interesting was also the difference in printing behavior and the achievable level of detail of the PMMA-free and PMMA-based feedstocks. Dental implants and the complex chess piece could be printed

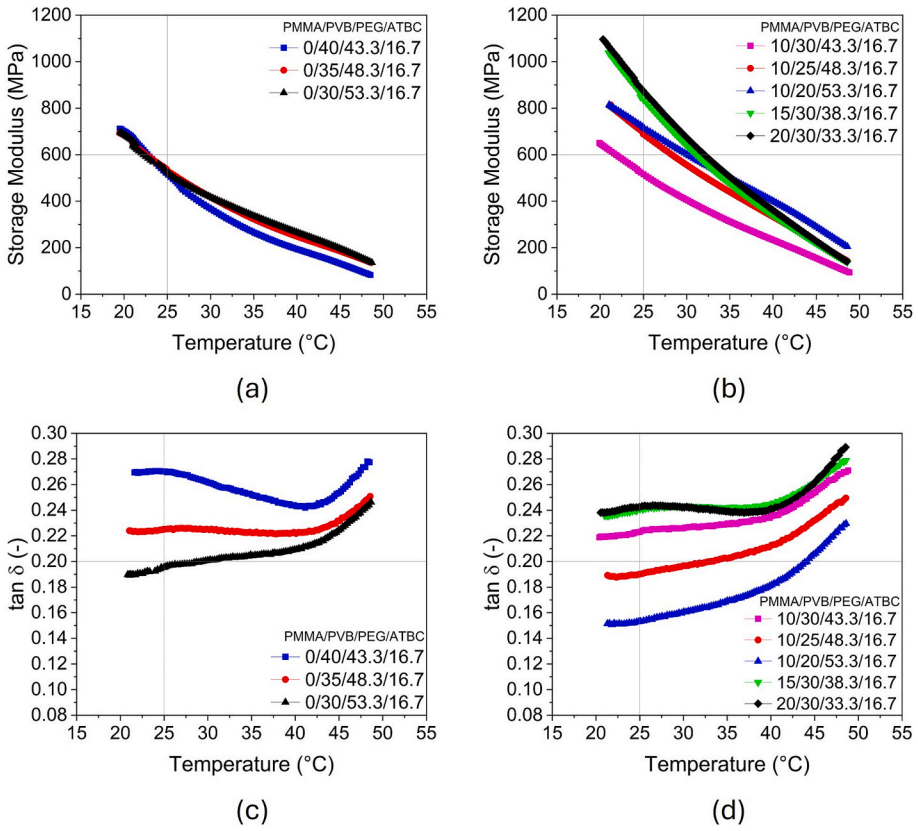

Fig. 5. Temperature sweeps of feedstocks made of PMMA/PVB/PEG/ATBC; (a) and (b) show the storage modulus, while the ratio of G″ and G′ is illustrated in (c) and (d).

Table 6
Overview of the printing temperature and the possible nozzle sizes.

PMMA/PVB/PEG/ATBC (vol.%)	Printing temperature (°C)	Bed temperature (°C)	Possible nozzle sizes (mm)
0/40/43.3/16.7	130	30	0.15–0.8
0/35/48.3/16.7	130	30	0.15–0.8
0/30/53.3/16.7	130	30	0.15–0.8
10/30/43.3/16.7	150	30–40	0.3–0.8
10/25/48.3/16.7	150	30–40	0.3–0.8
10/20/53.3/16.7	150	30–40	0.3–0.8
15/30/38.3/16.7	180	30–40	0.3–0.8
20/30/33.3/16.7	200	30–40	0.3–0.8

without any problems with the PMMA-free feedstocks due to the rapid solidification of PVB (Fig. 7a and b). However, the addition of PMMA increased the solidification time of the feedstocks. While this could be mitigated by reducing the printing speed to 3–4 mm/s for dental implants, the printing of the complex chess piece was only partly possible due to the shaking of the three strands by the figure when the print head deposited material (Fig. 7c and d). However, support structures with water-soluble materials could offer a viable solution to this challenge in the future. The use of larger nozzle sizes did not result in a significant decrease in the level of detail, but this could be a concern for even more delicate geometries.

3.4. Debinding and sintering

The debinding process was executed in a two-step procedure. To ensure fast and defect-free thermal debinding, open porosity is created in the samples by solvent debinding of PEG in water. Fig. 8a shows the pore fraction, calculated from the mass loss after solvent debinding, and

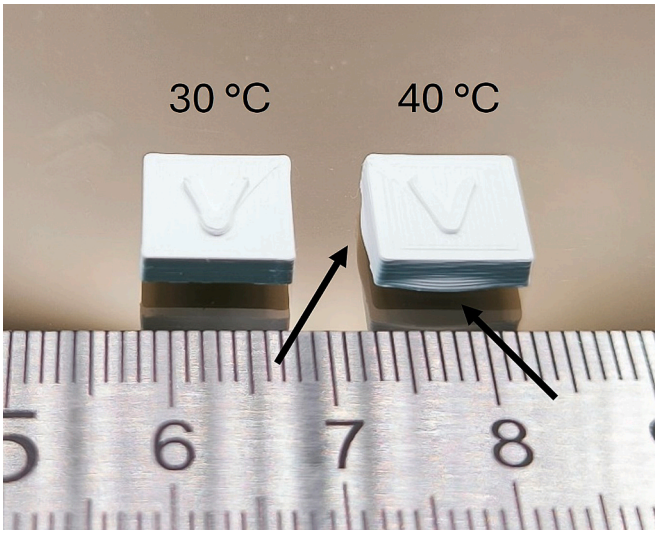

Fig. 6. Stable (30 °C) and deformed (40 °C) lower layers of the composition PMMA 0/PVB 40/PEG 43.3/ATBC 16.7. The arrows point to the deformations of the lower layers.

the relative density after sintering of the samples made from PMMA-free feedstocks. As the proportion of PEG in the binder increases, the pore fraction rises accordingly. Additionally, the steric blocking effect of the PVB chains and the strong hydrogen bonds between the PEG and the PVB chains are reduced. Due to their inability to form hydrogen bonds with one another, PEG chains are dependent on PVB chains. However, as the proportion of PEG increases and the proportion of PVB decreases, the number of hydrogen bonds formed decreases accordingly. Swelling and

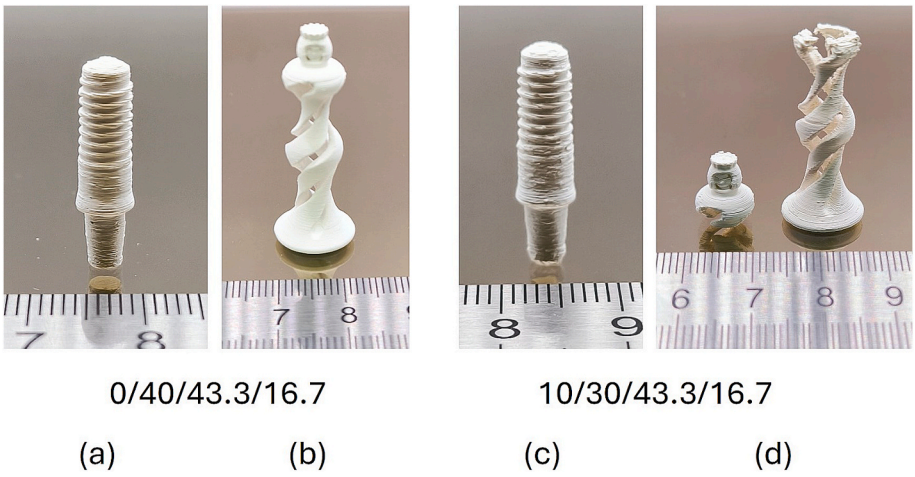

Fig. 7. Printed (a) dental implant and (b) chess queen with PMMA-free feedstock and printed (c) dental implant and (d) chess queen with PMMA-based feedstock (PMMA/PVB/PEG/ATBC).

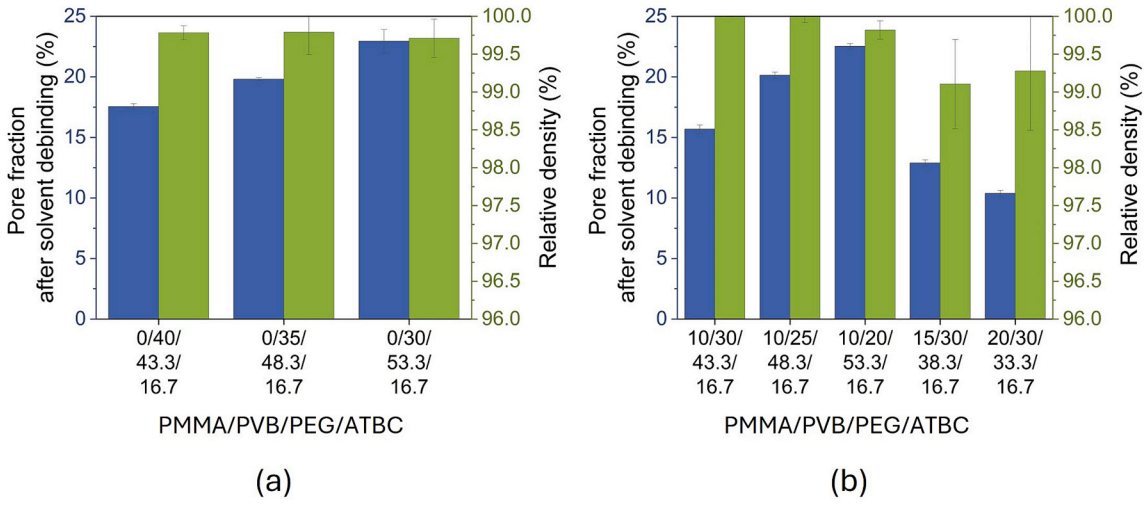

Fig. 8. (a) Pore fraction after solvent debinding and relative sinter density in samples made of PMMA/PVB/PEG/ATBC; (a) PMMA-free feedstocks and (b) PMMA-based feedstocks.

blistering was observed for all samples, but it became more distinct with increasing PEG content. This behavior is described in [28,39] and is related to the crystal structure of the PEG. The density of the final parts showed no significant differences between the three feedstocks, with values ranging from 99.5 % to 100.0 % across all samples. However, significant cracks were visible across all samples without the need for microscopic analysis. This observation can be attributed to the swelling of the PVB in water, leading to the delamination of some layers. This behavior likely hindered the attainment of higher relative densities. Partially substituting PVB with the water-resistant PMMA results in similar pore fractions in the samples (Fig. 8b). The reduced number of hydrogen bonds between the PVB chains is counterbalanced by a heightened steric blocking effect from the longer PMMA chains. However, replacing PEG with PMMA led to a significant decrease in open porosity, attributable to the reduced water-soluble PEG concentration in the samples and the enhanced blocking effects of backbone polymers. Blistering only occurred for the two feedstocks with a high PEG content. This observation is consistent with [39], but at lower PEG concentrations. This is likely due to the weaker bonding between the printed layers compared to homogeneous zirconia parts produced with injection molding and a binder system comprising PMMA and PEG [39]. High relative densities up to 100.0 % were attainable for the feedstocks containing 43.3 to 48.3 % PEG; however, large cracks were also visible for the feedstocks with 48.3 and 53.3 %, respectively. The other samples showed no visible defects. However, the two feedstocks with 15 and 20 % PMMA exhibited lower densities of approximately 99.0 to 99.3 %, with significant deviations. This behavior can be attributed to the high viscosity of the feedstocks and inhomogeneities, which may be caused by powder agglomerates present in them. These factors can lead to brief interruptions in the material flow during the printing process, which can result in defects. These defects are randomly distributed across all samples, contributing to the observed deviations.

The production of dental implants with all feedstocks, even those of high viscosity, was successfully achieved (Fig. 9a–d). However, manufacturing defect-free parts with complex geometries remains a challenge. While printing with PMMA-free feedstocks was possible, gravity-induced deformations during solvent debinding in water were observed (Fig. 9e). The addition of PMMA to the feedstocks effectively mitigated these deformations during the debinding step; however, it precluded the printing of the components with complex geometries (Fig. 9f).

3.5. *Microstructure*

As already indicated in the previous section, large cracks due to delamination were observed in five out of eight samples. Fig. 9 shows

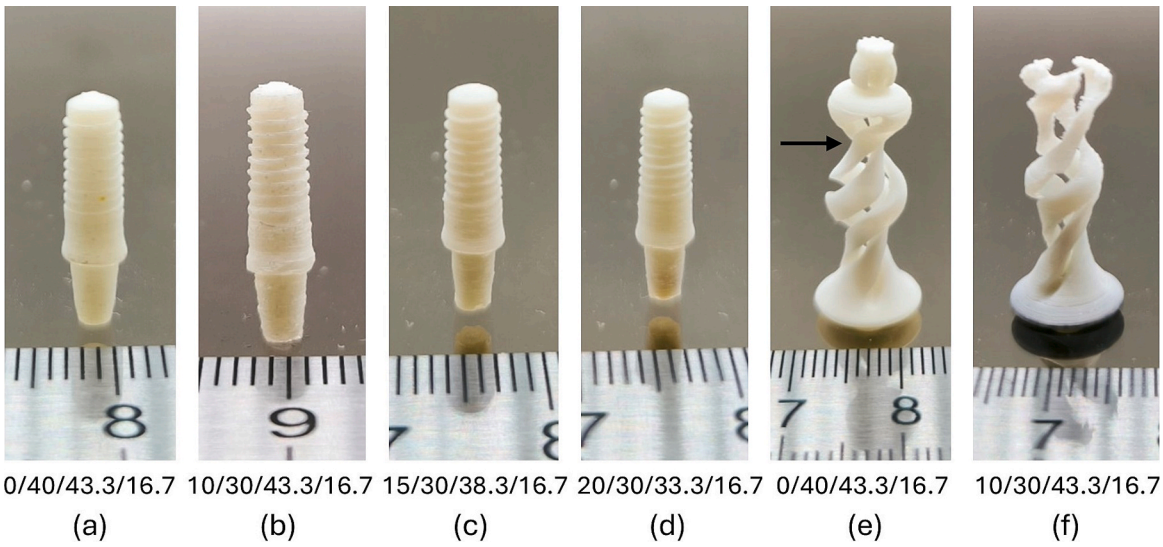

Fig. 9. Printed and sintered dental implants and chess figure produced with different binder compositions (PMMA/PVB/PEG/ATBC). The arrow in (e) shows the direction of the deformation of the chess piece made from a feedstock without PMMA.

SEM images of milled and polished cross-sections of six samples produced with six different feedstocks. For the PMMA-free feedstocks, large cracks can be seen throughout the entire sample (Fig. 10a and b). The assumption that these cracks originated from delamination of some layers is confirmed by Fig. 10b (0/30/53.3/16.7). It is evident that the crack path aligns with the surface structure, showcasing the layers' distinct morphology. Print related defects, as documented in [40], were not observed. By partially substituting PVB with PMMA, no visible defects were found in the sample in Fig. 10c (10/30/43.3/16.7), explaining the relative density of 100 %. The water-resistant PMMA prevented the swelling of the PVB, thereby suppressing the delamination of the layers. However, an increase in PEG led to a very straight crack through the entire sample (Fig. 10d). In comparison to PMMA-free feedstocks, only one crack was found in each sample. In contrast to [39], the cracks were found deep within the samples, rather than in close proximity to the surface. In such cases, the area where delamination occurs is likely the weakest point in the bonding between layers. Higher PMMA concentrations in combination with lower PEG contents prevented the formation of cracks (Fig. 10e and f). However, the elevated viscosity could lead to small defects during the printing process, thereby increasing the chance of defects in the samples and consequently reducing the average relative density.

4. Conclusion and outlook

The study examined eight distinct binder compositions to produce zirconia implants with no defects by CF^3, focusing on the flow behavior, the flexibility and the processibility of the feedstocks, as well as the

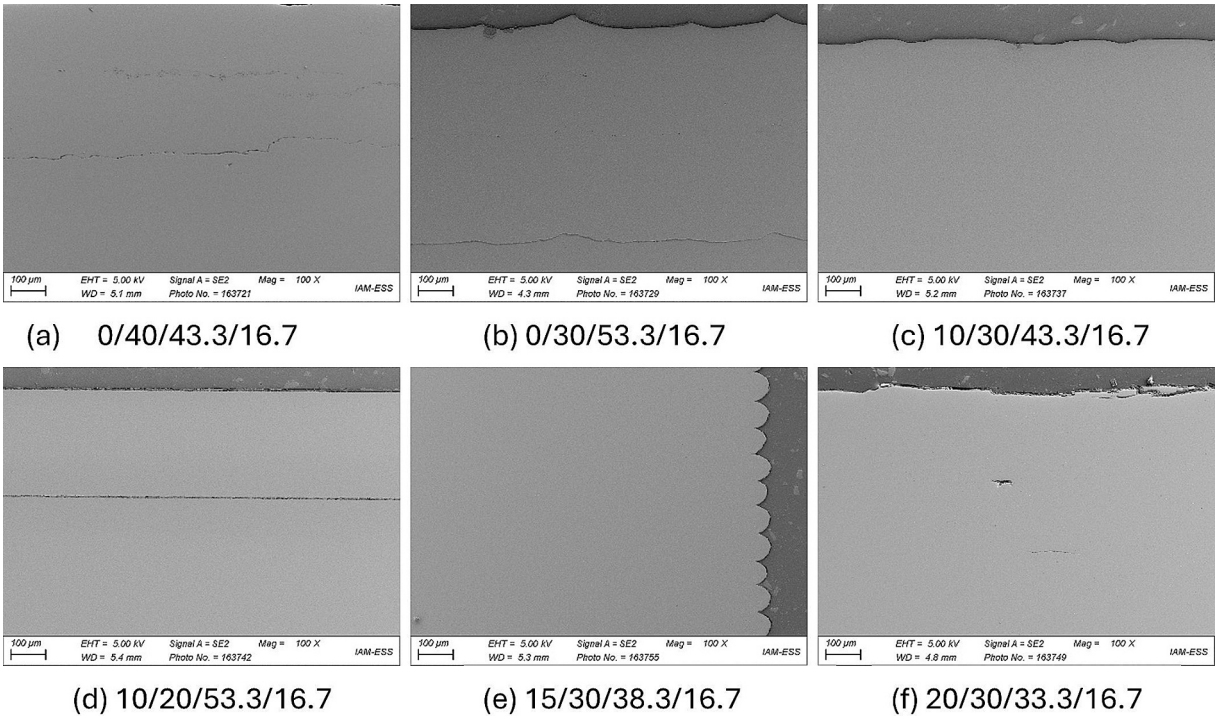

Fig. 10. SEM images of cross sections of the sintered cubic specimens produced with different binder compositions (PMMA/PVB/PEG/ATBC).

density and the microstructure of the final parts. The results indicated that feedstocks with PVB as the sole backbone polymer exhibited exceptional rheological and printing properties, ensuring a high level of usability. However, delamination during solvent debinding and the subsequent formation of cracks limit their application. The addition of PMMA to the feedstocks resulted in elevated viscosities, depending on the PMMA content, as well as slightly lower levels of detail in the printed parts. Furthermore, the slower solidification did not allow the printing of parts with very complex geometries. Nevertheless, PMMA could prevent the formation of cracks. The optimal feedstock system (10/30/43.3/16.7) demonstrated a relative density of 100 % without any defects.

Further studies will focus on milling the zirconia powder, destroying the aggregates and agglomerates, and ensuring better flow properties of the feedstocks. Additionally, a twin-screw extruder could be employed to improve agglomerate break and dispersion, thereby significantly accelerating the compounding process. It is also planned to examine the influence of PVB with higher acetalization degrees, which exhibit a higher water-resistance and therefore could prevent the swelling and delamination during the solvent debinding in water. In addition, biological cell tests will be carried out to investigate the proliferation on the produced ceramic implants. Finally, future research will also focus on applying the knowledge gained on other ceramic powders, such as alumina or hydroxyapatite.

CRediT authorship contribution statement

Ralf Eickhoff: Writing – review & editing, Writing – original draft, Visualization, Validation, Methodology, Investigation, Formal analysis, Conceptualization. **Dorit Nötzel:** Writing – review & editing, Validation, Supervision, Methodology. **Gülsenem Oral:** Writing – review & editing, Investigation. **Mark Scholz:** Writing – review & editing, Investigation. **Thomas Hanemann:** Writing – review & editing, Supervision, Resources, Project administration, Funding acquisition.

5. Funding

This research was supported by HEiKA. Open Access funding enabled and organized by Projekt DEAL.

Declaration of competing interest

The authors declare the following financial interests/personal relationships which may be considered as potential competing interests: Ralf Eickhoff reports financial support, administrative support, article publishing charges, and equipment, drugs, or supplies were provided by Karlsruhe Institute of Technology. Guelsenem Oral reports financial support was provided by Karlsruhe Institute of Technology. Mark Scholz reports financial support was provided by Karlsruhe Institute of Technology. Dorit Noetzel reports financial support, administrative support, article publishing charges, and equipment, drugs, or supplies were provided by Karlsruhe Institute of Technology. Thomas Hanemann reports financial support, administrative support, article publishing charges, and equipment, drugs, or supplies were provided by Karlsruhe Institute of Technology. Thomas Hanemann reports administrative support, article publishing charges, and equipment, drugs, or supplies were provided by University of Freiburg. Ralf Eickhoff reports a relationship with Karlsruhe Institute of Technology that includes: employment. Dorit Noetzel reports a relationship with Karlsruhe Institute of Technology that includes: employment. Guelsenem Oral reports a relationship with Karlsruhe Institute of Technology that includes: employment. Mark Scholz reports a relationship with Karlsruhe Institute of Technology that includes: employment. Thomas Hanemann reports a relationship with Karlsruhe Institute of Technology that includes: employment and travel reimbursement. Thomas Hanemann reports a relationship with University of Freiburg that includes: non-financial support and speaking and lecture fees. If there are other authors, they declare that they have no known competing financial interests or personal relationships that could have appeared to influence the work reported in this paper.

Acknowledgments

The authors thank the colleagues C. Odemer (KIT, Germany) for DSC/TG measurements and materialography, N. Bohn (KIT, Germany) for SEM images, M. Raab (KIT, Germany) for powder characterization and M. Engler and G. Link (KIT, Germany) for providing the DMA.

Data availability

The raw data of relevant measurements is available in Mendeley for open access at https://doi.org/10.17632/d9dntsd3h7.1.

References

[1] I. Buj-Corral, C. Herranz-Diez, A. Tejo-Otero, J. Otero, Biomedical applications of the fused filament fabrication (FFF) technology, in: Interaction of Nanomaterials With Living Cells, 2023, ch. Chapter 28, pp. 839–858.
[2] P. Wang, et al., Extrusion-based 3D co-printing: Printing material design and novel workflow for fabricating patterned heterogeneous tissue structures, Mater. Des. 227 (2023), https://doi.org/10.1016/j.matdes.2023.111737.
[3] M. Salmi, Additive manufacturing processes in medical applications, Materials (basel) 14 (1) (2021), https://doi.org/10.3390/ma14010191.
[4] Y. Zhu, et al., 3D printing biomimetic materials and structures for biomedical applications, Bio-Des. Manuf. 4 (2) (2021) 405–428, https://doi.org/10.1007/s42242-020-00117-0.
[5] B. Charbonnier, M. Hadida, D. Marchat, Additive manufacturing pertaining to bone: hopes, reality and future challenges for clinical applications, Acta Biomater. 121 (2021) 1–28, https://doi.org/10.1016/j.actbio.2020.11.039.
[6] Z. Chen, et al., 3D printing of ceramics: a review, J. Eur. Ceram. Soc. 39 (4) (2019) 661–687, https://doi.org/10.1016/j.jeurceramsoc.2018.11.013.
[7] H. Marcus, J. Beaman, J. Barlow, D. Bourell, Solid freeform fabrication an advanced manufacturing approach, Am. Ceram. Soc. Bull. 69 (1990).
[8] S. Bose, et al., 3D printing of ceramics: advantages, challenges, applications, and perspectives, J. Am. Ceram. Soc. 107 (12) (2024) 7879–7920, https://doi.org/10.1111/jace.20043.
[9] H. Li, L. Song, J. Sun, J. Ma, Z. Shen, Dental ceramic prostheses by stereolithography-based additive manufacturing: potentials and challenges, Adv. Appl. Ceram. 118 (1–2) (2018) 30–36, https://doi.org/10.1080/17436753.2018.1447834.
[10] C. Zhang, Z. Jiang, L. Zhao, W. Guo, X. Gao, Stability, rheological behaviors, and curing properties of 3Y–ZrO2 and 3Y–ZrO2/GO ceramic suspensions in stereolithography applied for dental implants, Ceram. Int. 47 (10) (2021) 13344–13350, https://doi.org/10.1016/j.ceramint.2021.01.191.
[11] M. Aldesoki, L. Keilig, I. Dorsam, B. Evers-Dietze, T.M. Elshazly, C. Bourauel, Trueness and precision of milled and 3D printed root-analogue implants: a comparative in vitro study, J. Dent. 130 (2023) 104425, https://doi.org/10.1016/j.jdent.2023.104425.
[12] A. Safonov, et al., Design and fabrication of complex-shaped ceramic bone implants via 3D printing based on laser stereolithography, Appl. Sci. 10(20) (2020). doi: 10.3390/app10207138.
[13] K. Sudan, P. Singh, A. Gökçe, V.K. Balla, K.H. Kate, Processing of hydroxyapatite and its composites using ceramic fused filament fabrication (CF3), Ceram. Int. 46 (15) (2020) 23922–23931, https://doi.org/10.1016/j.ceramint.2020.06.168.
[14] Z. Guan, X. Yang, P. Liu, X. Xu, Y. Li, X. Yang, Additive manufacturing of zirconia ceramic by fused filament fabrication, Ceram. Int. 49 (17) (2023) 27742–27749, https://doi.org/10.1016/j.ceramint.2023.05.230.
[15] M. Gauthé, et al., Fused filament fabrication of silicon carbide parts: a strategy for producing high-strength components, J. Eur. Ceram. Soc. 45(7) (2025). doi: 10.1016/j.jeurceramsoc.2025.117229.
[16] D. Nötzel and T. Hanemann, New feedstock system for fused filament fabrication of sintered alumina parts, Materials (Basel) 13(19) (2020). doi: 10.3390/ma13194461.
[17] K. Sudan, et al., Optimization of ceramic fused filament fabrication (CF3) for enhanced mechanical and biological properties of hydroxyapatite-silicon nitride biocomposites, Biomed. Mater. Devices (2025), https://doi.org/10.1007/s44174-025-00316-2.
[18] S. Esslinger, et al., Additive manufacturing of beta-tricalcium phosphate components via fused deposition of ceramics (FDC), Materials (Basel) 14(1) (2020). doi: 10.3390/ma14010156.
[19] J. Jacob, D. Pejak Simunec, A. E. Z. Kandjani, A. Trinchi, A. Sola, A review of fused filament fabrication of metal parts (metal FFF): current developments and future challenges, Technologies 12(12) (2024). doi: 10.3390/technologies12120267.
[20] J. Abel, et al., Fused filament fabrication (FFF) of metal-ceramic components, J. Vis. Exp. 143 (2019). doi: 10.3791/57693.

[21] C. Kukla, S. Cano, D. Kaylani, S. Schuschnigg, C. Holzer, J. Gonzalez-Gutierrez, Debinding behaviour of feedstock for material extrusion additive manufacturing of zirconia, Powder Metall. 62 (3) (2019) 196–204, https://doi.org/10.1080/00325899.2019.1616139.
[22] D. Nötzel, R. Eickhoff, T. Hanemann, Fused filament fabrication of small ceramic components, Materials (Basel) 11(8) (2018). doi: 10.3390/ma11081463.
[23] M. Vozárová, et al., Preparation of fully dense boron carbide ceramics by Fused Filament Fabrication (FFF), J. Eur. Ceram. Soc. 43 (5) (2023) 1751–1761, https://doi.org/10.1016/j.jeurceramsoc.2022.12.018.
[24] K.P.K. Ajjarapu, S. Barui, K. Sudan, S. Khanjar, K. Kate, Ceramic fused filament fabrication (CF3) of alumina: influence of powder particle morphology on processing and microstructure, Open Ceram. 19 (2024), https://doi.org/10.1016/j.oceram.2024.100631.
[25] S. Bhandari, et al., Ultra-rapid debinding and sintering of additively manufactured ceramics by ultrafast high-temperature sintering, J. Eur. Ceram. Soc. 44 (1) (2024) 328–340, https://doi.org/10.1016/j.jeurceramsoc.2023.08.040.
[26] F. Clemens, F. Sarraf, A. Borzì, A. Neels, A. Hadian, Material extrusion additive manufacturing of advanced ceramics: towards the production of large components, J. Eur. Ceram. Soc. 43 (7) (2023) 2752–2760, https://doi.org/10.1016/j.jeurceramsoc.2022.10.019.
[27] S. Cano, et al., Influence of the infill orientation on the properties of zirconia parts produced by fused filament fabrication, Materials (Basel) 13(14) (2020). doi: 10.3390/ma13143158.
[28] T. Heim, F. Kern, C. Siligardi, Influence of the binder composition on the water debinding properties of a PVB-PEG-alumina feedstock for the fused deposition of ceramic process, Open Ceram. 21 (2025), https://doi.org/10.1016/j.oceram.2024.100728.
[29] Implants for surgery – ceramic materials based on yttria-stabilized tetragonal zirconia (Y-TZP) (ISO 13356:2015), E. C. f. Standardization, 2015.
[30] A.C. Kutlu, D. Nötzel, C. Ziebert, H.J. Seifert, I. Ul Mohsin, 3D printing of Na1.3Al0.3Ti1.7(PO4)3 solid electrolyte via fused filament fabrication for all-solid-state sodium-ion batteries, Batter. Supercaps 7(1) (2023). doi: 10.1002/batt.202300357.
[31] R. Eickhoff, S. Antusch, D. Nötzel, M. Probst, T. Hanemann, Development of flexible and partly water-soluble binder systems for metal fused filament fabrication (MF3) of Ti-6Al-4V parts, Polymers 16(17) (2024). doi: 10.3390/polym16172548.
[32] T. Hanemann, R. Heldele, T. Mueller, J. Hausselt, Influence of stearic acid concentration on the processing of ZrO2-containing feedstocks suitable for micropowder injection molding, Int. J. Appl. Ceram. Technol. 8 (4) (2011) 865–872, https://doi.org/10.1111/j.1744-7402.2010.02519.x.
[33] R. Heldele, Entwicklung und Charakterisierung von Formmassen für das Mikropulverspritzgießen, Dissertation, Albert-Ludwigs-Universität Freiburg, Freiburg Im Breisgau (2008).
[34] M. Zurn, A. Schrage, S. Antusch, N. Bohn, P. Holzer, and T. Hanemann, Development of a polyethylene glycol/polymethyl methacrylate-based binder system for a borosilicate glass filler suitable for injection molding, Materials (Basel) 17(6) (2024). doi: 10.3390/ma17061396.
[35] R. Eickhoff, S. Antusch, S. Baumgartner, D. Nötzel, T. Hanemann, Feedstock development for material extrusion-based printing of Ti6Al4V parts, Materials 15 (18) (2022). doi: 10.3390/ma15186442.
[36] J.A. Naranjo, C. Berges, R. Campana, G. Herranz, Rheological and mechanical assessment for formulating hybrid feedstock to be used in MIM & FFF, Results Eng. 19 (2023), https://doi.org/10.1016/j.rineng.2023.101258.
[37] N. Venkataraman, et al., Feedstock material property – process relationships in fused deposition of ceramics (FDC), Rapid Prototyp. J. 6 (4) (2000) 244–253, https://doi.org/10.1108/13552540010373344.
[38] T. Beran, T. Mulholland, F. Henning, N. Rudolph, T.A. Osswald, Nozzle clogging factors during fused filament fabrication of spherical particle filled polymers, Addit. Manuf. 23 (2018) 206–214, https://doi.org/10.1016/j.addma.2018.08.009.
[39] X. Yang, C. Jia, Z. Xie, W. Liu, Q. Liu, Water-soluble binder system based on polymethyl methacrylate and poly-ethylene glycol for injection molding of large-sized ceramic parts, Int. J. Appl. Ceram. Technol. 10 (2) (2012) 339–347, https://doi.org/10.1111/j.1744-7402.2011.02745.x.
[40] D. Nötzel, R. Eickhoff, C. Pfeifer, T. Hanemann, Printing of zirconia parts via fused filament fabrication, Materials (Basel) 14(19) (2021). doi: 10.3390/ma14195467.